A BOMBARDMENT HISTROY OF THE MOON CONSTRAINED BY GRAIL-DERIVED POROSITY DATA.

Y. H. Huang[1], J. Soderblom[1], D. A. Minton[2], M. Hirabayashi[3], H. J. Melosh[2] [1]Department of Earth, Atmospheric, and Planetary Sciences, Massachusetts Institute of Technology, Cambridge, Massachusetts 02139, USA (yahuei@mit.edu), [2]Department of Earth, Atmopsheric, and Planetary Sciences, Purdue University, West Lafayette, Indiana 47907 USA, [3]Department of Aerospace Engineering, Auburn University, Auburn, Alabama 36849 USA.

Introduction: Understanding the impact history of the Solar System provides information about its dynamic evolution and the habitability of its planets [1, 2]. The Moon has the best of impact record in that it has been suject to little re-surfaceing. Radiometric ages derived from returned lunar samples allows us to establish a lunar absolute chronology [3]. The fact that the Moon is in a close proximity to Earth makes its impact record a critical constraint on the understanding of emergence of life on Earth. However, approaches to understanding an impact history of the Moon such as crater counting rely on the visibility of craters on a considered planetary surface. For ancient lunar highlands, using crater counting to recover its impact history becomes problematic due to crater counting equilibrium, in which craters are degraded [4].

Impact cratering can modify the subsurface of the planet [e.g., 5]. Extensive fracturing of basement materials results in a mass deficit surrounding terrestrial craters that are clearly seen in their gravity signature [5]. Fracturing and dilant bulking [6] are likely to be responsible for similar mass deficit found in lunar complex craters [7]. Recent modeling shows that for craters >100 km in diameter significant porosity is generated out nearly two radii beyond their rim due to tensile fragmentation [8]. On the other hand, when the target becomes sufficiently porous, impact cratering removes the porosity [6]. The relationship between compaction and porosity generation in subsurface is less studied.

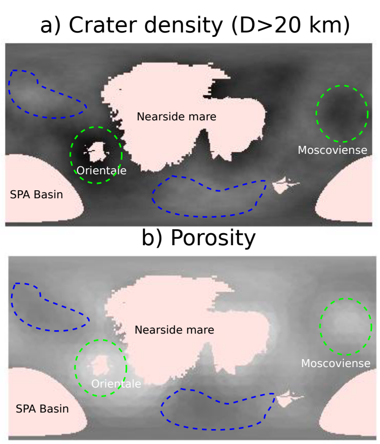

Figure 1: The lunar surface under cylindrical projection. We show a) N(20) map [12] and b) GRAIL-derived porosity map [11]. Orientale and Moscoviense Basins are outlined in green color, and the most heavily cratered surfaces are outlined in blue color. The brightness of the grayscale color represents the numeric value in N(20) and porosity.

Motivation: The Gravity Recovery and Interior Laboratory (GRAIL) mission [9] acquired the gravity fields of the Moon in unprecedented resolution, providing excellent data to understanding the porosity of the lunar crust [10, 11]. The GRAIL-derived porosity map reveals that the average bulk porosity of the lunar crust is ~10−12%, and that fractures may extend into the upper mantle in some regions [10]. The youngest basins on the Moon, such as Orientale and Moscoviense, has a high porosity in surrounding terrains while the most heavily cratered terrains, such as the southern nearside and central farside [12], has the lowest porosities (Figure 1).

Hypothesis: We propose a model to account for the relationship between cratering record and a planetary crust porosity. Large basins generate significant amount of porosity in the planet's crust and their surroundings extending out to some extent. Subsequent impacts compact the surface and subsurface, gradually removing the porosity over time. As a result, the observed porosity of a basin and its sourroundings reflects its cratering history.

Model: To test our hypothesis, we model the porosity of the lunar crust by assigning porosity values to each of basins and its surroundings. The youngst basin, Orientale, is assigned the highest observed porosity value (~18%) while the oldest basin, South Pole-Aitken, is assigned the lowest observed porosity value (~10%). We assign a specific porosity value to a basin based on their chronological order, so we account for the porosity generated by the formation of a basin and its destruction by subsequent cratering. Fourty-one basins (>300 km) are modeled and divided into 12 chronological orders using Wilhelms chronology [13]. The porosity of a basin transitions from the rim to the preexisting terrains gradually. The extent of the porosity of a basin and the size of a basin are parameters that we solve to match the observed porosity.

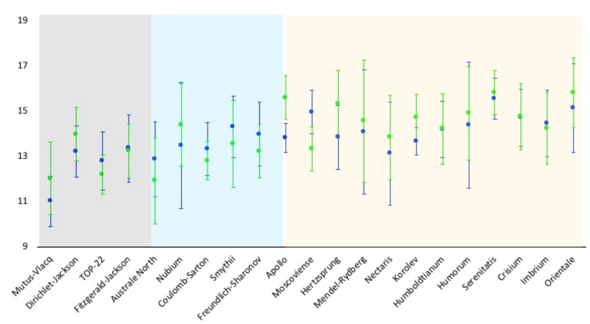

Figure 2: The porosity of large basins >400 km in diameter. The basin's name is shown at the x-axis with their modeled and observed porosity values shown at the y-axis. The circles in blue color represent mean observed porosity of basins, and the circles in green color represent our mean modeled porosity of basins. The bars are one standard deviation. The background colors, gray, light blue and light yellow, are to distinguish basins from GRAIL-discovered basins, Pre-Nectarian, and Nectarian and Imbrium, respectively. Overlapped basins such as Grimaldi and Cruger-Sirsalis Basins are excluded.

Results: Our modeled mean porosity of basins >400 km in diameter are within ~1−2% of observed porosities (Figures 2 and 3). The misfit of porosity in our model is caused by assigning incorrect chronology for a basin and lack of porosity interaction modeling between overlapped basins. For example, Moscoviense Basin is reported to be younger than Korolev and Mendel-Rydberg Basins in recent crater studies [14, 15]. We find that basins affect the porosity of the terrain 3.1±0.4 radii beyond their rims, which is consistent with the porosity profile we found for Orientale Basin (Figure 4). And the size of a basin that is primarily responsible for the lunar observed crustal porosity is 400 km in diameter. Our model shows that the GRAIL-discovered basins could be as old as SP-A because their observed porosity surrounding them is low. Some of the GRAIL-discovered basins are buried by younger basins, and their porosities are difficult to be recovered. For example, Cruger-Sirsalis Basin are surrounded by Orientale, Humorum, Grimaldi, and Mendel-Rydberg Basins.

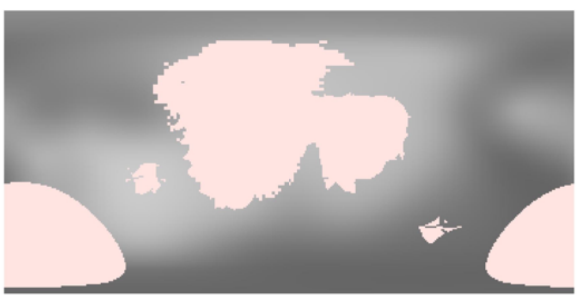

Figure 3: Our modeled lunar crustal porosity. The regions filled in pink color are Procellarum KREEP Terrane, SP-A, and the regions where density gradient is <5 kg/m³/km.

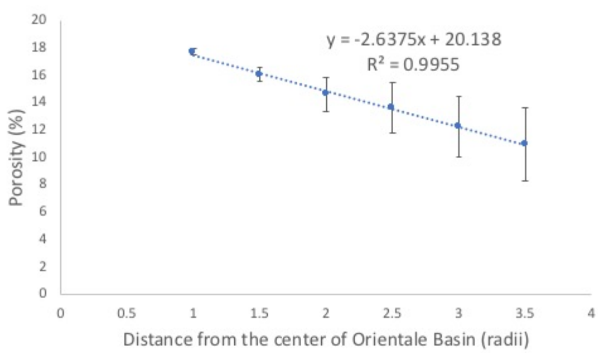

Figure 4: Porosity distribution of Orientale Basin. The x-axis is distance from the center of the basin, and the y-axis is observed porosity values. We binned the porosity into 0.5 radii bin. The squares in blue color are mean observed porosity with one standard deviation. The dashed line is linear function that fit into the mean observed porosity. The R^2 calculated by Excel provides a sense of how well the data fits the model.

Discussion: Our model suggests that the lunar crust porosity has not been crushed out in the entire impact bombardment history. The consequence of this enables us to interpret a cratering history of a basin in that the porosity of the basin initially generated is still preserved in the subsurface. The variation of porosity in basins is likely to reflect the amount of bombardment that they have received (Figure 2). Besides porosities of basins, the overall porosity of the lunar crust exhibits a dependence on cratering history (Figure 5). In high porosity terrains (14−18%), the porosity decreases linearly with N(20). As the terrain reaches porosity of <14%, their N(20) becomes flatten out due to crater saturation. However, the porosity appears to continue to decrease to ~9%. If the linear decrease seen in the high porosity region can be applied to the lower porosity region, it suggests that the rate of compaction linearly relates to the number of craters. For the most cratered terrains, the southern nearside and central farside, we predict the total craters >20 km in diameter of >410 needed to reach this lowest porosity.

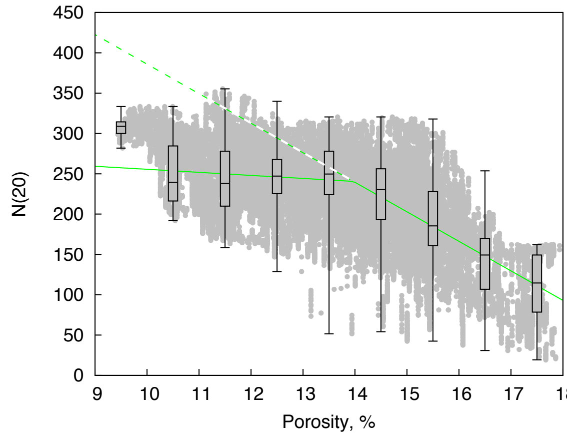

Figure 5: The observed porosity and the number of craters >20 km in diameter, N(20). The box and whisker plot is obtained by binning all observed porosity into 1% porosity bins. The lines inside of the box is the median value of the observed porosity at given bin. The upper and lower boundaries of the box represent the 25% of data above the median and the 25% of data below the median, respectively. The ends of the whisker represent the maximum and minimum. The green solid lines are fitting slopes at the breakpoint ~14%. The dashed green line is extrapolated from the fitting slope that we obtained for the porosity range between 14% and 18%.

References: [1] Cockell, C. S. *Philos. Trans. R. Soc. B Biol. Sci.*, 361, 1845-1855, (2006). [2] Gomes, R., et al. *Nature*, 435, 466-469, (2005). [3] Neukum, G. et al., *Space Sci. Rev*., 96, 55-86, (2001). [4] Gault, D. E., *Radio Sci.*, 5(2), 273-291, (1970). [5] Pilkington, M. and Grieve, R. A. F., *Rev. Geophys.*, 30, 161-181, (1992). [6] Milbury, C. et al. *Geophys. Res. Lett.*, 42, 9711-9716, (2015). [7] Soderblom, J. M. et al., *Geophys. Res. Lett.*, 42, 6939-6944, (2015). [8] Wiggins, S. E., et al., *J. Geophys. Res. Planets*, 124, 9941-957, (2019). [9] Zuber, M., et al., *Science* 339, 668-671, (2013). [10] Wieczorek, M., et al., *Science* 339, 671-676, (2013). [11] Besserer, J. et al., *Geophys. Res. Lett.*, 41, 5771-5777, (2014). [12] Head, J. et al., *Science* 329, 1504-1507, (2010). [13] Wilhelms, D. E., *U.S. Geol. Surv. Prof. Pap.* 1348, 283-292, (1987). [14] Orgel, C., et al., *J. Geophys. Res. Planets*, 123, 748-762, (2018). [15] Fassett, C. I., et al. *J. Geophys. Res.* 117, E00H06, (2012).